Structural properties of glassy Ge_2Se_3 from first-principles molecular dynamics

Sébastien Le Roux, Assil Bouzid, Mauro Boero, and Carlo Massobrio
Institut de Physique et de Chimie des Matériaux de Strasbourg, 23 rue du Loess, BP43, F-67034 Strasbourg Cedex 2, France
(Received 31 July 2012; revised manuscript received 11 October 2012; published 19 December 2012)

The structural properties of glassy Ge_2Se_3 were studied in the framework of first-principles molecular dynamics by using the Becke-Lee-Yang-Parr scheme for the treatment of the exchange-correlation functional in density functional theory. Our results for the total neutron structure factor and the total pair distribution function are in very good agreement with the experimental results. When compared to the structural description obtained for liquid Ge_2Se_3, glassy Ge_2Se_3 is found to be characterized by a larger percentage of fourfold coordinated Ge atoms and a lower number of miscoordinations. However, Ge−Ge homopolar bonds inevitably occur due to the lack of Se atoms available, at this concentration, to form $GeSe_4$ tetrahedra. Focusing on the family of glasses Ge_xSe_{1-x}, the present results allow a comparison to be carried out in reciprocal and real space among three prototypical glassy structures. The first was obtained at the stoichiometric composition (glassy $GeSe_2$), the second at a Se-rich composition (glassy $GeSe_4$) and the third at a Ge-rich composition (glassy Ge_2Se_3). All networks are consistent with the "$8-N$" rule, in particular, glassy $GeSe_4$, which exhibits the highest degree of chemical order. The electronic structure of glassy Ge_2Se_3 has been characterized by using the Wannier localized orbital formalism. The analysis of the Ge environment shows the presence of dangling, ionocovalent Ge−Se, and covalent bonds, the latter related to Ge−Ge connections.

DOI: 10.1103/PhysRevB.86.224201 PACS number(s): 61.43.Fs, 61.25.Em, 61.20.Ja, 71.15.Pd

I. INTRODUCTION

The atomic structure of the glasses Ge_xSe_{1-x} (or g-Ge_xSe_{1-x} in what follows) for $0 \leqslant x \leqslant 0.33$ can be viewed as the result of a continuous transition from a Se-rich phase (small x values), encompassing Se chains interconnected with $GeSe_4$ tetrahedra, to a full $GeSe_4$ tetrahedral network highly chemically ordered ($x = 0.33$), i.e., glassy $GeSe_2$. Moving to the $x \geqslant 0.33$ side of the composition range, g-Ge_xSe_{1-x} are known to form up to $x \leqslant 0.43$, a representative example being provided by g-Ge_2Se_3. A comparative analysis of diffraction data for g-Ge_xSe_{1-x} revealed that g-Ge_2Se_3 shares some notable features with g-$GeSe_3$, g-$GeSe_2$, and g-$GeSe_4$.[1] One can mention, in reciprocal space, the existence of a prepeak at $k \sim 1$ Å^{-1} in the number-number Bhatia-Thornton partial structure factor, indicative of intermediate range order. In real space, the corresponding Bhatia-Thornton number-number partial pair distribution function exhibits a very intense peak at ∼2.4 Å and a broader maximum at ∼4 Å, much in the same way as g-$GeSe_3$, g-$GeSe_2$, and g-$GeSe_4$.[1] Also, the mean coordination number of g-Ge_2Se_3 (2.81) is consistent with the value expected from the "$8-N$" rule where Ge atoms are fourfold coordinated and Se atoms are twofold coordinated. In spite of these pieces of evidence and in the absence of measurements of the full set of partial structure factors, the atomic topology of g-Ge_2Se_3 is far from being well understood. For instance, no information is available on the chemical nature and the percentages of the structural motifs (such as n-fold Ge and Se atoms).

In this paper, we apply first-principles molecular dynamics (FPMD) to the study of structural properties of g-Ge_2Se_3. Our ultimate intent is to compare a number of relevant properties (partial structure factors, pair correlation functions, coordination numbers, nature, and percentages of structural motifs) calculated for g-Ge_2Se_3, liquid Ge_2Se_3 (l-Ge_2Se_3) g-$GeSe_2$, and g-$GeSe_4$. Complete structural characterizations of l-Ge_2Se_3, g-$GeSe_2$, and g-$GeSe_4$ have been performed in recent years by using FPMD in conjunction with various recipes for the exchange-correlation functionals.[2–12]

Within this context, we take advantage of the availability of an extended set of FPMD trajectories produced for liquid Ge_2Se_3 to obtain g-Ge_2Se_3 at $T = 300$ K by rapid quenching from temperatures in the liquid state. Our comparative analysis follows a twofold strategy, namely the description of the structural modifications (a) when going from the liquid to the glass for a given composition ($x = 0.4$) and (b) with changing composition ($x = 0.2,\ 0.33,\ 0.4$) within the g-Ge_xSe_{1-x} family.

The paper is organized as follows. Our theoretical model is described in Sec. II. The results for the neutron total structure factor and the total pair correlation function of g-Ge_2Se_3 are presented and compared to the experimental data in Sec. III. The reciprocal space properties (Faber-Ziman and Bhatia-Thornton partial structure factors) are given in Sec. IV. Section V is devoted to the real-space properties (pair distribution functions, coordination numbers and structural units). In both Secs. IV and V, the comparison extends to g-Ge_2Se_3, l-Ge_2Se_3, g-$GeSe_2$, and g-$GeSe_4$. In Sec. VI, we focus on some relevant features of the electronic structure, such as the electronic density of states and the orbital analysis in terms of the maximally localized Wannier functions (this latter section is devoted to the specific case of configurations extracted from the temporal trajectories of l-Ge_2Se_3 and g-Ge_2Se_3 only). Finally, the conclusions are summarized in Sec. VII.

II. THEORETICAL MODEL

Our simulations were performed on a system containing $N = 120$ (48 Ge and 72 Se) atoms in a periodically repeated cubic cell of size 15.21 Å, corresponding to the experimental density of the glass at 300 K, $\rho_{exp} = 4.3271$ g cm^{-3}.[1] Very recently, for the prototypical case of liquid $GeSe_2$, we have demonstrated that the changes occurring when increasing the

system size from $N = 120$ to 480 do not alter the essence of the structural information obtained for the smaller system. We concluded that calculations performed at $N = 120$ are as reliable as those carried out for $N = 480$.[7]

The electronic structure was described in the framework of density functional theory (DFT) with the generalized gradient approximation (GGA) due to Becke (B) for the exchange energy and Lee, Yang, and Parr (LYP) for the correlation energy.[13,14] The method by Car and Parrinello was employed to ensure a self-consistent evolution of the electronic structure during the molecular dynamics motion.[15] The BLYP approach was chosen since it proved to give a better description of short-range properties (especially in the case of Ge-Ge interactions) in a Ge-Se networks where the tetrahedral coordination is predominant (liquid and glassy $GeSe_2$).[3,5,16,17] In particular, we refer to Ref. 5 for a detailed account of the reasons underlying the better performances of the BLYP approach when compared to the Perdew and Wang scheme.[18] Concerning the setup of the simulations and the comparison between the present results (for g-Ge_2Se_3) and those relative to other concentrations (for g-$GeSe_2$ and g-$GeSe_4$), two additional points are worth reminding. The data presented of g-$GeSe_2$ have been obtained by averaging the quantities over two new trajectories generated at $T = 300$ K (BLYP functional) within the NVT and the NPT ensemble at ambient conditions ($T = 300$ K and zero pressure), respectively. This new set of results on g-$GeSe_2$ improve upon those of Ref. 3. In the case of g-$GeSe_4$ instead, we exploit published results for the pair correlation functions and the partial structure factors obtained in the Perdew-Wang framework.[4] However, for sake of consistency, an additional run in the BLYP framework was also produced and employed to compare the coordination numbers and the electronic density of states (see below). While a complete assessment of the effect of the BLYP functional on the structural properties of g-$GeSe_4$ is out of the scope of the present study, this strategy is beneficial to achieve an optimal comparison between g-$GeSe_2$, g-$GeSe_4$, and g-Ge_2Se_3.

In our work, the valence electrons were treated explicitly, in conjunction with norm-conserving pseudopotentials of the Trouiller-Martins type to account for core-valence interactions.[19] The wave functions were expanded at the Γ point of the supercell on a plane-wave basis set with an energy cutoff $E_c = 20$ Ry. A fictitious electron mass of 2000 a.u. (i.e., in units of $m_e a_0^2$, where m_e is the electron mass and a_0 is the Bohr radius) and a time step of $\Delta t = 0.24$ fs are adopted to integrate the equations of motion. Temperature control was implemented for both the ionic and electronic degrees of freedom by using Nosé-Hoover thermostats.[20–22]

To prepare ten g-Ge_2Se_3 samples, ten initial configurations fully decorrelated and separated by 10 ps were provided by our recent study of the liquid Ge_2Se_3.[6] For each one of these subtrajectories, we proceeded as follows to quench the Ge_2Se_3 liquid: (a) the density of the initial liquid configuration at $T = 1000$ K was set to the one of the amorphous state,[1] (b) the modified Ge_2Se_3 system was equilibrated at $T = 1000$ K for 10 ps, and (c) the thermostat temperature was set to $T = 900$, 600, and 300 K, with annealing over periods of time equal to 20, 30, and 50 ps, respectively. Finally, statistical averages were taken over each subtrajectory covering a total time interval of 52 ps at $T = 300$ K. In the following, the results presented for glassy Ge_2Se_3 are calculated by taking the mean over the set of ten averaged data resulting from the corresponding subtrajectories. Typical error bars are of the order of a few percents.

For g-Ge_2Se_3, the electronic density of states (EDOS) has been produced by extracting ten independent configurations from each one of the ten subtrajectories. This leads to a total of 100 configurations contributing to the statistical average. For comparative purposes, and whenever they were not already available in the literature, we have also calculated the EDOS at other concentrations by adopting the same concept of sampling uncorrelated configurations (typically 50–100).

Analysis of the detailed electronic structure is given in term of the maximally localized Wannier functions.[23,24] Following the standard procedure, the Wannier functions and the corresponding centers are obtained as unitary transformation *on the fly* of the Kohn-Sham orbitals. Specifically, among all the possible unitary transformation, we select the one minimizing the spread

$$\Omega = \sum_i (\langle i|\mathbf{r}^2|i\rangle - \langle i|\mathbf{r}|i\rangle^2). \tag{1}$$

This leads to an iterative scheme for computing the orbital transformation

$$w_n(\mathbf{r}) = \sum_i \left[\prod_p \exp\left(-A_{i,n}^p\right) \psi_i(\mathbf{r})\right], \tag{2}$$

where p is the order of the iteration as specified in Ref. 23. The Wannier states provide in this way an unbiased method for partitioning the charge density and the electronic information becomes then contracted into four numbers, the center of the orbital,

$$x_n = -\frac{L}{2\pi} \Im m \ln\langle w_n|\exp(-i2\pi x/L)|w_n\rangle \tag{3}$$

with similar expressions along the other two cartesian directions, and its related spread. Here, L is the length of the simulation cell along the x direction.

III. NEUTRON TOTAL STRUCTURE FACTOR AND TOTAL PAIR CORRELATION FUNCTION

The total neutron structure factor $S_T(k)$ is defined by

$$S_T(k) - 1 \equiv \sum_{\alpha=1}^{n}\sum_{\beta=1}^{n} \frac{c_\alpha c_\beta b_\alpha b_\beta}{\langle b\rangle^2}\left[S_{\alpha\beta}^{FZ}(k) - 1\right], \tag{4}$$

where α and β denote the chemical species, $n = 2$ is the number of different chemical species, c_α and b_α are the atomic fraction and coherent neutron scattering length of chemical species α, $\langle b\rangle = c_{Ge}b_{Ge} + c_{Se}b_{Se}$ is the mean coherent neutron scattering length, and $S_{\alpha\beta}^{FZ}(k)$ is a Faber-Ziman (FZ) partial structure factor. The coherent neutron scattering lengths for Ge and Se of natural isotopic abundance are $b_{Ge} = 8.185$ fm and $b_{Se} = 7.970$ fm.[1] In real space, the corresponding quantity is the total pair distribution function:

$$\begin{aligned} g_T(r) - 1 &= \frac{1}{2\pi^2 n_0 r}\int_0^\infty dk\, k\, [S_T(k) - 1]\, \sin(kr) \\ &= \sum_{\alpha=1}^{n}\sum_{\beta=1}^{n} \frac{c_\alpha c_\beta b_\alpha b_\beta}{\langle b\rangle^2}[g_{\alpha\beta}(r) - 1], \end{aligned} \tag{5}$$

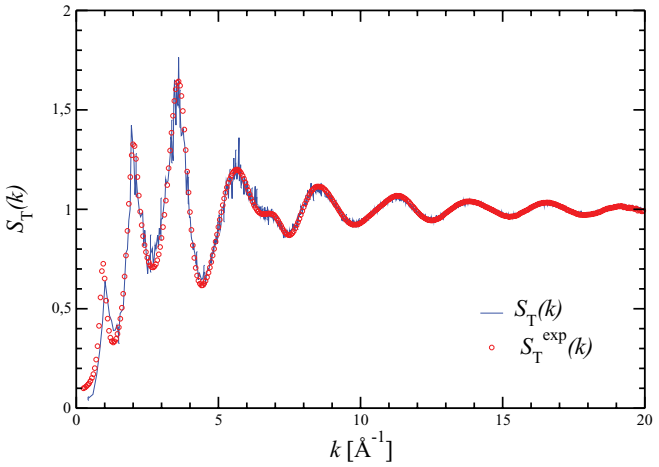

FIG. 1. (Color online) Total neutron structure factor for amorphous Ge_2Se_3 at $T = 300$ K. The experimental result $S_T^{exp}(k)$ given in Ref. 25 (red circles) is compared to the calculated function $S_T^{th}(k)$ (solid blue curve). For sake of clarity, only a representative subset of error bars are given at specific location in the reciprocal space.

where n_0 is the atomic number density and $g_{\alpha\beta}(r)$ is a partial pair distribution function. The total neutron structure factor $S_T^{th}(k)$ is presented in Fig. 1 along with its experimental counterpart $S_T^{exp}(k)$.[25] The agreement is very good over the entire range of wave vectors as shown by the observation that the position and the intensity of the peaks are well reproduced.

The measured and calculated total pair distribution functions for g-Ge_2Se_3 are compared in Fig. 2. The experimental result, $g_T^{exp}(r)$, was obtained by Fourier transforming the reciprocal space data set with an upper limit of integration set to $k_{max} = 19.95$ Å^{-1} in Eq. (5). This upper limit results from the finite measurement window function of the diffractometer and leads to spurious oscillations at $r < 2$ Å. We obtain

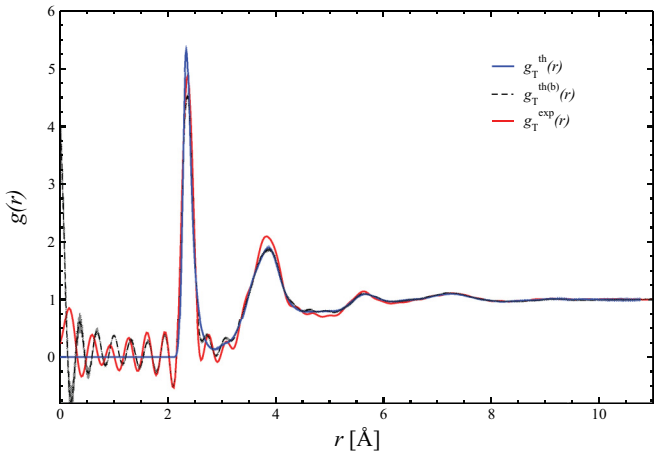

FIG. 2. (Color online) Total pair distribution function for amorphous Ge_2Se_3 at $T = 300$ K. The experimental function $g_T^{exp}(r)$ of Ref. 25 (solid red line) was obtained by Fourier transforming the measured total structure factor $S_T^{exp}(k)$ (see Fig. 1) with a cutoff value $k_{max} = 19.95$ Å^{-1}. The same procedure was applied to the computed function $S_T^{th}(k)$ (see Fig. 1) to obtain $g_T^{th(b)}(r)$ (broken black curve). The total pair distribution function $g_T^{th}(r)$ (solid blue curve) is the result of a direct calculation from the real-space coordinates.

the total pair distribution function from the FPMD results in two different manners. In the first, the function $g_T^{th}(r)$ was calculated directly from the atomic coordinates of the simulation. In the second, the experimental procedure was followed such that the calculated total structure factor $S_T^{th}(k)$ was Fourier transformed with $k_{max} = 19.95$ Å^{-1} to give the function $g_T^{th(b)}(r)$. As a result, the first main peak of $g_T^{th(b)}(r)$ turns out to be closer to $g_T^{exp}(r)$ than $g_T^{th}(r)$. The total pair correlation function $g_T^{th}(r)$ is not affected by the oscillating behavior in the interval 2.5Å $< r <$ 3.5 Å but it differs slightly from experiments in the intensity of the peak located at ∼4 Å. Remarkably, the small bump present at 5.5 Å is accurately reproduced by both $g_T^{th}(r)$ and $g_T^{th(b)}(r)$.

IV. RECIPROCAL SPACE PROPERTIES

A. Faber-Ziman partial structure factors

The calculated Faber-Ziman (FZ) partial structure factors for g-Ge_2Se_3 are shown in Fig. 3 where a comparison is made with the analogous quantities obtained for g-$GeSe_2$, g-$GeSe_4$, and l-Ge_2Se_3. First, we shall focus on the changes occurring on quenching liquid Ge_2Se_3 to produce g-Ge_2Se_3. In the partial structure factors $S_{SeSe}^{FZ}(k)$ and $S_{GeSe}^{FZ}(k)$ there is an increase of the peak intensities. A notable exception is the small shoulder in the prepeak region ($k \sim 1$ Å^{-1}) of $S_{GeSe}^{FZ}(k)$, insensitive to the decrease of temperature. This means that the impact of Ge-Se next-nearest neighbors correlations on the intermediate range order is quite limited for both liquid and glassy Ge_2Se_3. A different situation is encountered for $S_{GeGe}^{FZ}(k)$. Both l-Ge_2Se_3 and g-Ge_2Se_3 feature an important contribution of Ge-Ge correlations to the intermediate range order. However, the ratio $R_{FSDP/Main}$ between the intensities of the first two peaks (first sharp diffraction peak and the main peak) increases in g-Ge_2Se_3, as a sign of enhanced Ge-Ge intermediate range correlation in the glassy case.

Despite the important statistical noise in the case of g-$GeSe_2$ and g-$GeSe_4$, an increase of $R_{FSDP/Main}$ is also noticeable in $S_{GeGe}^{FZ}(k)$ for increasing Ge content, since $R_{FSDP/Main}$ is larger in g-Ge_2Se_3 than in g-$GeSe_4$. Comparison between the three cases (g-$GeSe_2$, g-$GeSe_4$, and g-Ge_2Se_3) is indicative of a smoother profile in the FSDP region of $S_{GeGe}^{FZ}(k)$ for g-Ge_2Se_3, owing to the larger number of Ge atoms and the better statistics (24 Ge atoms in g-$GeSe_4$, 40 in g-$GeSe_2$, and 48 in g-Ge_2Se_3). The most intense main peak ($k \sim 2$ Å^{-1}) in $S_{GeSe}^{FZ}(k)$ occurs for g-$GeSe_2$. On the contrary, the largest intensity for the feature at $k \sim 1$ Å^{-1} in $S_{GeSe}^{FZ}(k)$ is found in the g-$GeSe_4$ case. Finally, in the case of $S_{SeSe}^{FZ}(k)$, the main peak has a reduced intensity for g-$GeSe_4$. This correlates well with the smaller number of Se atoms participating in $GeSe_4$ tetrahedra for this composition. In a way consistent with this observation, the intensity of this same peak is similar in $GeSe_2$ and Ge_2Se_3.

B. Bhatia-Thornton partial structure factors

In Fig. 4, we compare the Bhatia-Thornton (BT) number-number, $S_{NN}(k)$, number-concentration, $S_{NC}(k)$, and concentration-concentration, $S_{CC}(k)$, partial structure factors[27,28] for g-$GeSe_2$, g-$GeSe_4$, g-Ge_2Se_3, and l-Ge_2Se_3.

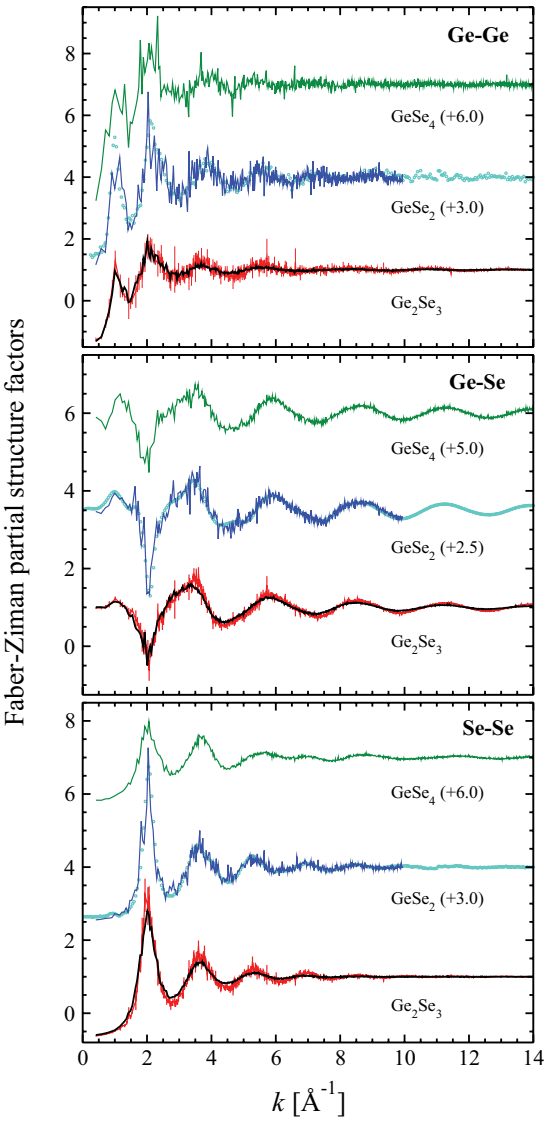

FIG. 3. (Color online) The Faber-Ziman partial structure factors $S^{FZ}_{GeGe}(k)$ (top), $S^{FZ}_{GeSe}(k)$ (middle), and $S^{FZ}_{SeSe}(k)$ (bottom) for g-Ge_2Se_3 (present work, solid red lines), l-Ge_2Se_3 (from Ref. 6, solid black lines), g-$GeSe_2$ (from Ref. 26, solid blue lines), and g-$GeSe_4$ (from Ref. 4, solid green lines). Experimental counterpart for g-$GeSe_2$ is also presented (from Ref. 1, light blue dots).

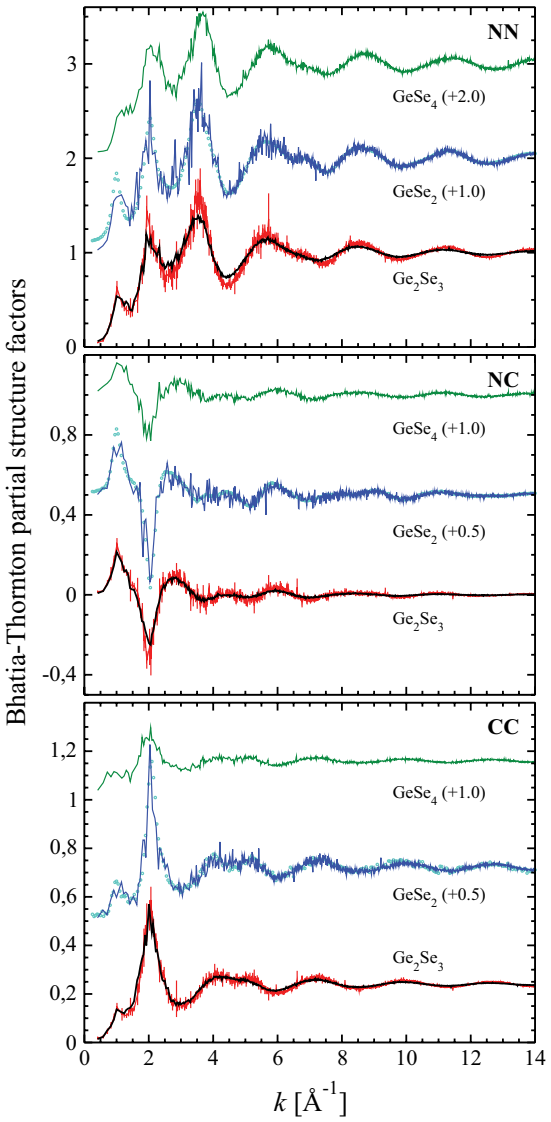

FIG. 4. (Color online) The Bhatia-Thornton partial structure factors $S_{NN}(k)$ (top), $S_{NC}(k)$ (middle), and $S_{CC}(k)$ (bottom) for g-Ge_2Se_3 (present work, solid red lines), l-Ge_2Se_3 (from Ref. 6, solid black lines), g-$GeSe_2$ (from Ref. 26, solid blue lines), and g-$GeSe_4$ (from Ref. 4, solid green lines). Experimental counterpart for g-$GeSe_2$ is also presented (from Ref. 1, light blue dots).

In terms of the Bhatia-Thornton partial structure factors, the total neutron structure factor reads

$$S_T(k) = S_{NN}(k) + A\,[S_{CC}(k)/c_{Ge}\,c_{Se} - 1] + B\,S_{NC}(k), \quad (6)$$

where $A = c_{Ge}c_{Se}\Delta b^2/\langle b\rangle^2$, $B = 2\Delta b/\langle b\rangle$, and $\Delta b = b_{Ge} - b_{Se}$.[29]

$S_T(k)$ is a very good approximation for $S_{NN}(k)$, i.e., $|S_T(k) - S_{NN}(k)| < 0.025$. This is due to the fact that, at least for the compositions $c_{Ge} = 0.2, 0.33, 0.4$, the coefficients $A \lesssim 1.0\times10^{-4}$ and $B \lesssim 0.054$ due to the similarity between the scattering lengths of Ge and Se (8.185 and 7.970, respectively). In consequence, the consideration developed for $S_T(k)$ shown in Fig. 1 hold equally well for $S_{NN}(k)$ shown in Fig. 4.

The $S_{NC}(k)$ and FZ partial structure factors are related by the expression

$$S_{NC}(k) = c_{Ge}c_{Se}\{c_{Ge}[S^{FZ}_{GeGe}(k) - S^{FZ}_{GeSe}(k)] - c_{Se}[S^{FZ}_{SeSe}(k) - S^{FZ}_{GeSe}(k)]\}, \quad (7)$$

while the relationship between $S_{CC}(k)$ and the FZ partial structure factors is as follows:

$$S_{CC}(k) = c_{Ge}c_{Se}(1 + c_{Ge}c_{Se}\{[S^{FZ}_{GeGe}(k) - S^{FZ}_{GeSe}(k)] + [S^{FZ}_{SeSe}(k) - S^{FZ}_{GeSe}(k)]\}). \quad (8)$$

The BT partial structure factors do not undergo any major change from l-Ge_2Se_3 to g-Ge_2Se_3, having similar patterns and differing only in the intensities of the main peaks, in line with what found in the FZ case.

When comparing the BT partial structure factors for the three glasses, a positive contribution to $S_{NC}(k)$ appears coming from the $c_{Ge}S^{FZ}_{GeGe}(k)$ term in the FSDP region. This term is less important in g-$GeSe_4$ than in g-$GeSe_2$ and g-Ge_2Se_3 due to the smaller concentration of Ge atoms and the reduced intensity of the FSDP in $S^{FZ}_{GeGe}(k)$ for the case of g-$GeSe_4$. Among the partial structure factors $S_{CC}(k)$ under considerations, the most distinguishable features in the FSDP region can be found for g-$GeSe_2$, g-Ge_2Se_3, and l-Ge_2Se_3. In the past, the presence of this feature was associated to a small and yet non-negligible departure from chemical order.[30] Accordingly, chemical disorder is expected to be less important in g-$GeSe_4$ than in g-$GeSe_2$, g-Ge_2Se_3, and l-Ge_2Se_3.[30]

Globally, two kinds of conclusions can be drawn from the reciprocal space data. For the given Ge_2Se_3 network, liquid and glassy systems share the same patterns in the partial structure factors. Due to the high quench rate, it might be argued that this observation is trivial and could be the mere byproduct of the glass production method. However, this is not the case, since our strategy was capable of accounting for differences in reciprocal space for other pairs of chalcogenide liquids and glasses.[4,5] Changes in concentration and in the coordination of Ge and Se atoms can be correlated with differences in the absolute and relative intensities of the FSDP (at $k \sim 1$ Å^{-1}) and the first main peak (at $k \sim 2$ Å^{-1}).

V. REAL-SPACE PROPERTIES

A. Pair distribution functions

In Fig. 5, we display the calculated partial pair distribution functions $g_{\alpha\beta}(r)$ for g-Ge_2Se_3 together with the calculated functions for l-Ge_2Se_3.[3] The pair distribution functions for g-$GeSe_2$ and g-$GeSe_4$ are also given.

For g-Ge_2Se_3, the main peak in $g_{GeSe}(r)$ is much sharper and higher than in the l-Ge_2Se_3 case. This observation confirms the persistence of a predominant Ge centered tetrahedral motif in the glassy state. Besides the increased intensity of the main peak, the partial structure factors $g_{SeSe}(r)$ differ by the disappearance in the glass of any discernible feature at distances characteristic of Se−Se homopolar bonds. The decrease in the number of homopolar connections on cooling was recorded in the case of g-$GeSe_2$ and does correspond to the disruption of homopolar bonds kept together by thermal activation only on very short-time intervals.[4]

In Ref. 6, the pair distribution function $g_{GeGe}(r)$ of l-Ge_2Se_3 was described in terms of one visible peak (the one at $r = 2.47$ Å, which arises from Ge−Ge homopolar bonds) and a broad feature extending in between 3 and 4.5 Å. This second maximum was postulated to be due to edge-sharing motifs at a distance $r \simeq 3$ Å and corner-sharing motifs at larger distances. A quench from the liquid was intended as a method to obtain a clear resolution of the edge-sharing and corner-sharing contributions, in line with other studies on Ge_xSe_{1-x} systems.[3,31] The suggestion of Ref. 6 finds a confirmation in the present results, since a three peak structure appears in g-Ge_2Se_3 after cooling. Interestingly, the lack of available Se atoms to form tetrahedral connections has the effect of largely preserving the role of Ge–Ge homopolar bonds, not bound to disappear upon cooling as seen in the case of Se atoms.

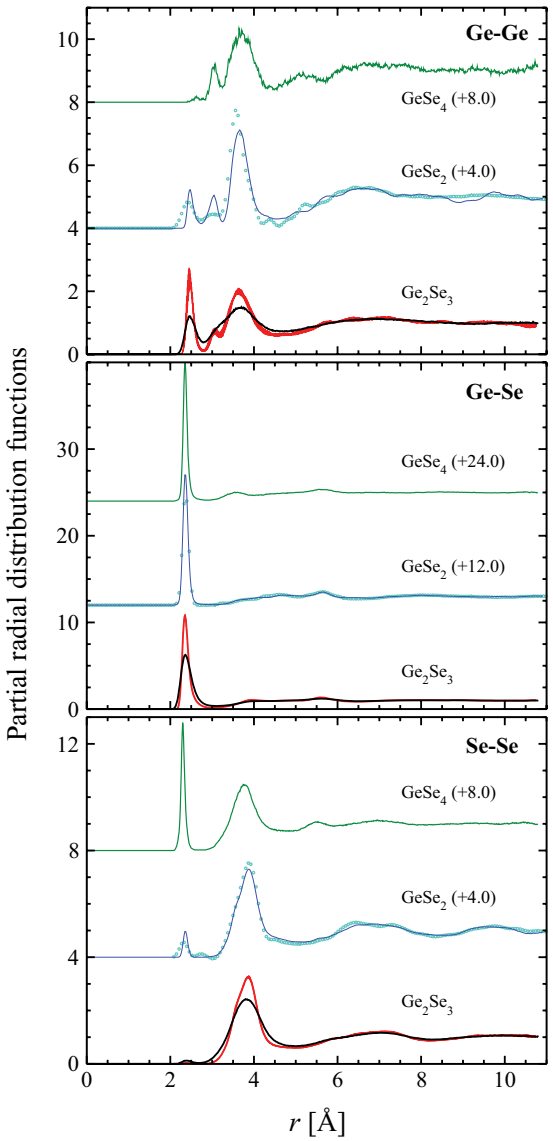

FIG. 5. (Color online) The partial pair distribution functions $g_{GeGe}(r)$ (top), $g_{GeSe}(r)$ (middle), and $g_{SeSe}(r)$ (bottom) for g-Ge_2Se_3 (present work, solid red lines), l-Ge_2Se_3 (from Ref. 6, solid black lines), g-$GeSe_2$ (from Ref. 26, solid blue lines), and g-$GeSe_4$ (from Ref. 4, solid green lines). Experimental counterpart for g-$GeSe_2$ is also presented (from Ref. 1, light blue dots).

It is of interest to follow the trend of $g_{\alpha\beta}(r)$ for changing composition. The case of $g_{GeSe}(r)$ is most likely the simplest to capture, since the very intense main peak is a measure of the predominance of the tetrahedral $GeSe_4$ coordination. Moving to the $g_{SeSe}(r)$ case, relevant changes are found for $r \sim 2.4$–2.5 Å as a result of different numbers of Se−Se connections, each one indicative of a specific topology. However, while Se−Se connections are inevitable in g-$GeSe_4$, they also appear in g-$GeSe_2$ as a sign of a (small) deviation from chemical order. The pair distribution functions $g_{GeGe}(r)$ relative to g-$GeSe_2$, g-Ge_2Se_3, and g-$GeSe_4$ share a three-peak structure, well known for being indicative of homopolar bonds, edge-sharing and corner-sharing tetrahedra. The relative proportion of these

TABLE I. The first-peak position (FPP) and second-peak position (SPP) in $g_{\alpha\beta}(r)$ and the nearest-neighbor coordination numbers $\bar{n}_{\alpha\beta}$ obtained from FPMD models of g-Ge_2Se_3 (present work), l-Ge_2Se_3, g-$GeSe_2$, and g-$GeSe_4$.[4,6,26] The coordination numbers $\bar{n}_{\alpha\beta}$ for g-Ge_2Se_3 were obtained by using an integration range of 0–2.9 Å where the upper limit corresponds to the first minimum in the total pair distribution function. The predictions of the CON and RCN models are also listed.[1]

$g_{\alpha\beta}(r)$	model	FPP (Å)	SPP (Å)	$\bar{n}_{\alpha\beta}$	$\bar{n}_{\alpha\beta}$ (CON)	$\bar{n}_{\alpha\beta}$ (RCN)
$g_{GeGe}(r)$	g-$GeSe_4$	2.64	3.65	0.01	2	1.3333
	g-$GeSe_2$	2.47	3.67	0.28	0	2
	g-Ge_2Se_3	2.47	3.63	0.52	1	2.2857
	l-Ge_2Se_3	2.47	3.70	0.48	1	2.2857
$g_{GeSe}(r)$	g-$GeSe_4$	2.36	3.54	3.92	4	2.6667
	g-$GeSe_2$	2.34		3.84	4	2
	g-Ge_2Se_3	2.35	5.61	3.21	3	1.7143
	l-Ge_2Se_3	2.36	5.65	3.15	3	1.7143
$g_{SeGe}(r)$	g-$GeSe_4$	2.36	3.54	0.98	1	0.6666
	g-$GeSe_2$	2.34		1.82	2	1
	g-Ge_2Se_3	2.35	5.61	2.14	2	1.1429
	l-Ge_2Se_3	2.36	5.65	2.10	2	1.1429
$g_{SeSe}(r)$	g-$GeSe_4$	2.29	3.76	1.01	1	1.3333
	g-$GeSe_2$	2.34	3.76	0.2	0	1
	g-Ge_2Se_3	2.37	3.88	0.01	0	0.8571
	l-Ge_2Se_3	2.39	3.81	0.08	0	0.8571

motifs is highly dependent on the composition, as proved by the little bump at the Ge−Ge homopolar bonds location in g-$GeSe_4$. This feature becomes an unmistakable peak in g-$GeSe_2$ (a sign of the deviation from chemical order) and a peak of larger intensity in g-Ge_2Se_3, owing to the presence of those Ge atoms that cannot form tetrahedra with Se atoms on the Ge-rich side of the composition range.

B. Coordination numbers

The coordination numbers $\bar{n}_{\alpha\beta}$ of g-$GeSe_2$, g-$GeSe_4$, g-Ge_2Se_3, and l-Ge_2Se_3 are listed in Table I. They are defined as the mean number of nearest neighbors of type β around an atom of type α within an integration range that includes distances up to the first minimum of the total pair distribution function. The values of $\bar{n}_{\alpha\beta}$ are the quantitative counterpart of the observations compiled above for the partial pair distribution functions. In particular, it appears that $\bar{n}_{GeGe}$ is higher in g-Ge_2Se_3 and in l-Ge_2Se_3 than in g-$GeSe_2$ and g-$GeSe_4$, as a result of the presence of Ge atoms not tetrahedrally coordinated to Se atoms. Worth of note is also the decrease of $\bar{n}_{SeSe}$ in g-Ge_2Se_3 when compared to l-Ge_2Se_3 (0.01 against 0.08), i.e., Se chains have almost disappeared. In Table I, we also provide the values of $\bar{n}_{\alpha\beta}$ associated with two simple models for the network structure of disordered Ge_xSe_{1-x}. In the chemically ordered network (CON) model, Ge−Se bonds are favored such that only Ge−Se and Ge−Ge bonds are allowed for compositions with $x > 0.33$, while only Ge−Se and Se−Se bonds are allowed for compositions with $x < 0.33$. In the random covalent network (RCN) model there is a purely statistical distribution of bond types such that Se−Se bonds are allowed for $x < 0.33$ and Ge−Ge bonds are allowed for $x > 0.33$. While it appears clearly that the RCN model does not describe any of the glasses under consideration, the CON model provides an acceptable prediction for the structure of g-$GeSe_4$, as shown particularly by the values of $\bar{n}_{GeGe}$ and $\bar{n}_{SeSe}$. CON is less reliable for g-$GeSe_2$ and g-Ge_2Se_3. For instance, the calculated $\bar{n}_{GeGe}$ values larger and smaller, respectively, than those predicted by the CON model.

The total coordination numbers for Ge and Se are given by $\bar{n}_{Ge} = \bar{n}_{GeGe} + \bar{n}_{GeSe}$ and $\bar{n}_{Se} = \bar{n}_{SeSe} + \bar{n}_{SeGe}$, respectively, where $\bar{n}_{SeGe}/c_{Ge} = \bar{n}_{GeSe}/c_{Se}$. The average coordination number irrespective of chemical species type is given by the expression $\bar{n} = c_{Ge}(\bar{n}_{GeGe} + \bar{n}_{GeSe}) + c_{Se}(\bar{n}_{SeSe} + \bar{n}_{SeGe})$. A comparison is also made with the measured $\bar{n}$ values and with the $\bar{n}$ values expected from the "$8 - N$" rule where Ge atoms are fourfold coordinated and Se atoms are twofold coordinated. We recall that both the CON and the RCN model can be compatible with this rule, intrinsically unable to discriminate between two structures differing in the amount of chemical order. Table II shows that all systems follow the "$8 - N$" rule

TABLE II. The total coordination numbers for Ge, $\bar{n}_{Ge}$, and Se, $\bar{n}_{Se}$, in g-Ge_2Se_3 as calculated by using a cutoff distance of 2.9 Å. The results are compared with those obtained from FPMD models of the l-Ge_2Se_3 g-$GeSe_2$ and g-$GeSe_4$ (Refs. 4,6,26). The calculated average coordination number $\bar{n}$ for each system is also listed and the values are compared with the experimental results of Ref. 1 and with the expectations of the "$8 - N$" rule. PW and BLYP identify two distinct exchange-correlation functionals employed in the case of g-$GeSe_4$.

Model	$\bar{n}_{Ge}$	$\bar{n}_{Se}$	$\bar{n}$	$\bar{n}$(exp)	$\bar{n}$("$8 - N$")
g-$GeSe_4$(BLYP)	3.96	2.01	2.40	2.44	2.4
g-$GeSe_4$(PW)	3.93	1.99	2.37	2.44	2.4
g-$GeSe_2$	3.92	2.02	2.66	2.69	2.67
g-Ge_2Se_3	3.73	2.15	2.78	2.81(5)	2.8
l-Ge_2Se_3	3.63	2.18	2.76	2.8(2)	2.8

TABLE III. Generalized Warren-Cowley and the Cargill-Spaepen short-range chemical order parameters for g-Ge_2Se_3 (present work), l-Ge_2Se_3, g-$GeSe_2$, and g-$GeSe_4$.[4,6,26] The parameters are normalized (see the text) and are compared to the values expected from the "$8-N$" rule. PW and BLYP identify two distinct exchange-correlation functionals employed in the case of g-$GeSe_4$.

Model	α_w^0	η^0	α_w^0 (CON)	α_w^0 (RCN)	η^0 (CON)	η^0(RCN)
g-$GeSe_4$(BLYP)	0.19	0.90	0.219	− 0.042	1	0
g-$GeSe_4$(PW)	0.20	0.99	0.219	− 0.042	1	0
g-$GeSe_2$	0.78	0.86	1.0	− 0.125	1	0
g-Ge_2Se_3	0.72	0.99	0.519	− 0.099	1	0
l-Ge_2Se_3	0.73	0.92	0.519	− 0.099	1	0

quite accurately. At this level of comparison, the results for g-$GeSe_4$ are proved not to be sensitive to the choice of the functional ($\bar{n}_{PW} = 2.37$, $\bar{n}_{BLYP} = 2.40$).

In Ref. 6, we have employed a specific methodology to explore the ordering of disordered systems at different compositions. This amounts to an exploration of the generalized Warren-Cowley[32,33] and the Cargill-Spaepen[34] short-range chemical order parameters defined by $\alpha_w \equiv 1 - \bar{n}_{GeSe}/c_{Se}\bar{n}_w$ and $\eta \equiv \bar{n}_{GeSe}\bar{n}/c_{Se}\bar{n}_{Ge}\bar{n}_{Se} - 1$, respectively, where $\bar{n}_{GeSe}/c_{Se} = \bar{n}_{SeGe}/c_{Ge}$ and $\bar{n}_w = c_{Se}\bar{n}_{Ge} + c_{Ge}\bar{n}_{Se}$. It is also convenient to define the normalized order parameters $\alpha_w^0 = \alpha_w/\alpha_w^{max}$ and $\eta^0 = \eta/\eta^{max}$ where the superscript max corresponds to the case when, for fixed composition and coordination numbers $\bar{n}_{Ge}$ and $\bar{n}_{Se}$, the heteropolar coordination number is a maximum such that either $\bar{n}_{Ge} = \bar{n}_{GeSe}$ with $\bar{n}_{GeGe} = 0$ or $\bar{n}_{Se} = \bar{n}_{SeGe}$ with $\bar{n}_{SeSe} = 0$. The normalization parameters are given by $\eta^{max} = c_{Se}\bar{n}_{Se}/c_{Ge}\bar{n}_{Ge}$ if $c_{Ge}\bar{n}_{Ge} > c_{Se}\bar{n}_{Se}$ or $\eta^{max} = c_{Ge}\bar{n}_{Ge}/c_{Se}\bar{n}_{Se}$ if $c_{Ge}\bar{n}_{Ge} < c_{Se}\bar{n}_{Se}$ (see Ref. 34), while $\alpha_w^{max} = 1 - \bar{n}_{Ge}/c_{Se}\bar{n}_w$ if $c_{Ge}\bar{n}_{Ge} > c_{Se}\bar{n}_{Se}$ or $\alpha_w^{max} = 1 - \bar{n}_{Se}/c_{Ge}\bar{n}_w$ if $c_{Ge}\bar{n}_{Ge} < c_{Se}\bar{n}_{Se}$.[35] The chemical order parameters for g-$GeSe_2$, g-$GeSe_4$, g-Ge_2Se_3, and l-Ge_2Se_3 are given in Table III, where a comparison is also made with the values expected for the CON and the RCN models. Based on these parameters, the highest level of chemical order has to attributed to g-$GeSe_4$, this conclusion not being affected by the choice of the exchange-correlation functional for this system. Both g-$GeSe_2$ and g-Ge_2Se_3 (as well as l-Ge_2Se_3) are more chemically disordered than g-$GeSe_4$.

C. Structural units and network topology

To provide a more complete description of the network we identify the individual α-l structural units where an atom of species α (Ge or Se) is l-fold coordinated to other atoms. Within this notation, Ge-$GeSe_3$ represents a Ge atom that is connected to one other Ge atom and three Se atoms while Ge-Se_4 represents a Ge atom that is connected to four Se atoms. The proportion of a specific unit $\bar{n}_\alpha(l)$ is found by taking the ratio of the mean number of its occurrences to the total number of atoms of type α. Bonds are deemed to be formed when the interatomic distance for a given pair of atoms is smaller than 2.9 Å, corresponding to the first minimum in the total pair distribution function, a choice that is consistent with the analysis carried out for g-$GeSe_2$.[2,36,37] The proportions of l-fold coordinated atoms and of each specific unit $\bar{n}_\alpha(l)$ are presented in Figs. 6 and 7. Figure 6 presents results of the calculation for g-Ge_2Se_3 (present work) and l-Ge_2Se_3 (from Ref. 6), whereas Fig. 7 presents results of the calculation for g-$GeSe_2$ and g-$GeSe_4$.[4,26] As a first observation of Fig. 6, we note that the number of fourfold Ge atoms is larger in g-Ge_2Se_3 than in l-Ge_2Se_3 (by about 10 %), mostly at the expenses of twofold Ge atoms, strongly reduced in g-Ge_2Se_3 (from 9.65 % in the liquid to 3.52 % in the glass). The same effect is visible in the Se case, with an increase (by 5 %) in g-Ge_2Se_3 of twofold Se atoms at the expenses of (miscoordinated) threefold Se atoms. We recall that the twofold Ge atoms present in l-Ge_2Se_3 were characterized by very reduced average lifetimes, determined from the average number of consecutive configurations of a given kind.[6] It appears that upon cooling such a lifetime essentially vanishes, decreasing the importance of the twofold units. In turn, this also favors the increase of the predominant structural unit (the fourfold connection) for which lower activation barriers have to be overcome. In Fig. 6, one notices that in g-Ge_2Se_3 the number of Se atoms miscoordinated (onefold, threefold, fourfold) are reduced with respect to l-Ge_2Se_3, leading to ∼85% of Se atoms twofold coordinated.

On the Ge-rich side of the Ge_xSe_{1-x} composition range (g-$GeSe_4$) and at the stoichiometric composition (g-$GeSe_2$), the tetrahedral coordination is highly predominant and, more specifically, the undefective $GeSe_4$ tetrahedron (see Fig. 7). This holds in particular for g-$GeSe_4$, in line with our previous analysis based on the coordination numbers and the chemical order parameters. The number of Se atoms twofold coordinated is larger than 90%. An interesting difference in this respect exists between g-$GeSe_4$ and g-$GeSe_2$. In g-$GeSe_2$ more than 80% of the twofold Se atoms have two Ge atoms as nearest neighbors. This stems from the topology of the network in which Se−Se chains are rare. A different distribution among the Se-Se-Se, Ge-Se-Ge, and Se-Se-Ge (termed BB, AA, and BB in Ref. 4) connections is found in g-$GeSe_4$, this corresponds to fully interconnected Se chains and $GeSe_4$ tetrahedra.

Finally, it is of interest to classify the Ge atoms by counting those belonging to at least one fourfold ring, Ge_{edge}. The labeling "edge," identifies these atoms as being connected (or not) in an edge-sharing fashion, all the other Ge atoms being in corner-sharing or homopolar configurations. The lowest percentage of Ge_{edge} atoms is found for g-$GeSe_4$ (22%), followed by g-$GeSe_2$ (35%), g-Ge_2Se_3 (41%) and l-Ge_2Se_3 (45%). Overall the number of Ge_{edge} atoms increases with the proportion of Ge atoms. These conclusions supersede those drawn in Ref. 6 where the relative intensity of the first maximum in the Ge-Se-Ge bond angle distribution was claimed to be proportional to the percentage of edge-sharing connections. Indeed, this correlation does not hold in the

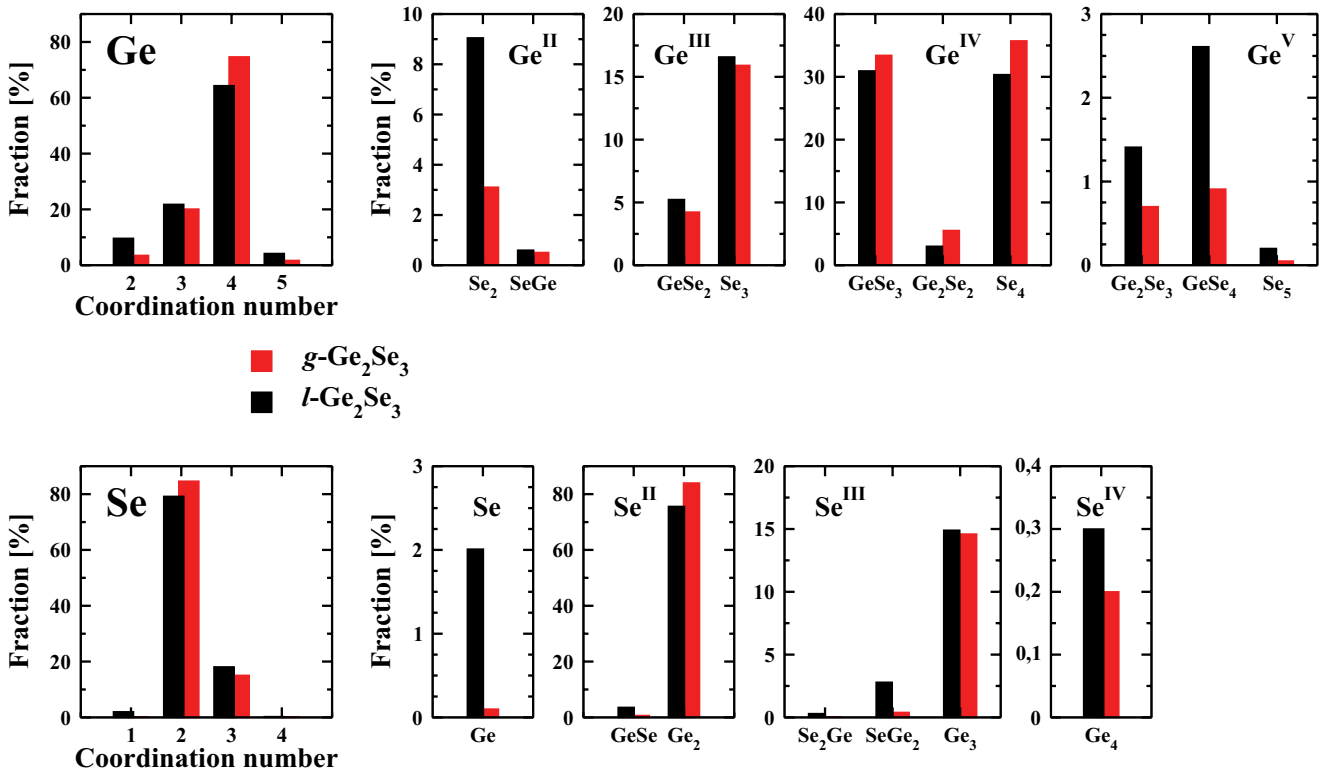

FIG. 6. (Color online) Percentage of l-fold coordinated atoms, also decomposed in term of each specific unit $\bar{n}_\alpha(l)$, for both Ge (top) and Se (bottom). The systems considered are g-Ge_2Se_3 (in red, present work) and l-Ge_2Se_3 (in back, from Ref. 6).

presence of an important number of chemically disordered fourfold rings (containing homopolar Ge-Ge bonds). According to our definition, these rings contribute to the counting of Ge atoms belonging to at least one fourfold ring, but they are not necessarily associated to Ge-Se-Ge triads. This is exactly the case of glassy and liquid Ge_2Se_3 thereby explaining why the number of Ge in fourfold rings and the height of the first peak in the the Ge-Se-Ge bond angle distribution are, respectively, higher and lower than in the $GeSe_2$ case.

VI. ELECTRONIC PROPERTIES

A comprehensive view of the electronic density of states (EDOS) for g-Ge_2Se_3, l-Ge_2Se_3, g-$GeSe_2$, and g-$GeSe_4$ is given in Fig. 8. Focusing on the Ge_2Se_3 networks, the EDOS of g-Ge_2Se_3 has a much deeper pseudogap around the Fermi level than l-Ge_2Se_3, in spite of the fact that the main structural features of g-Ge_2Se_3 and l-Ge_2Se_3 are similar. Therefore this difference indicates that the tendency toward a metallic character found in l-Ge_2Se_3 has a dynamical nature and manifests itself through frequent bond breaking and restoring processes, absent or much less frequent in g-Ge_2Se_3. In the vicinity of the Fermi level, the patterns followed by the EDOS of g-$GeSe_2$ and g-Ge_2Se_3 are quite similar, a small gap opening up for g-$GeSe_2$. When comparing the EDOS of g-$GeSe_4$ for two different functionals (PW and BLYP), a striking difference stands out in the behavior around the Fermi level. The pseudogap becomes markedly deeper in the BLYP case, by conferring to the BLYP g-$GeSe_4$ an electronic character similar to the one of g-$GeSe_2$ and g-Ge_2Se_3 and, most importantly, closer to experimental evidence.[38,39] This result is in line with previous studies on the performance of the PW and BLYP functional in the case of g-$GeSe_2$ and l-$GeSe_2$.[5,16] The BLYP approach gave an improved structural description due to a better account of electron localization effects, partially correcting the overestimate of the metallic character inherent to DFT approaches based on the local density approximation and to a lesser extent, the PW scheme.

The evolution of the electronic structure has been monitored in terms of maximally localized Wannier function centers (WFCs). In this paragraph we shall focus on peculiar features characterizing l-Ge_2Se_3 and g-Ge_2Se_3 during and after the formation of chemical bonds. In the case of l-Ge_2Se_3, the network evolves dynamically, with continuous disruption and formation of chemical bonds. A couple of features, specific to the liquid phase, are shown in the snapshots of Fig. 9. In particular (left panel), we provide an example of the environment around two Ge atoms attempting to form a homopolar bond. The two atoms termed Ge_1 and Ge_2 are separated by a distance of 2.69 Å, hence larger than standard Ge–Ge bonds (∼2.43 Å). A single WFC, indicated as W_4, is located at a very short distance (0.31 Å) from Ge_2 with a spread of 2.89 Å. The small distance and the large spread are indicative of both a dangling bond (DB) and a Ge–Ge bond formation process, as it will be further elucidated in the ongoing discussion relative to g-Ge_2Se_3. When Ge–Se bonds are present, as shown in the same panel, the characteristic ionic character of the system is preserved. In fact the $Ge_1 - W_1$, $Ge_1 - W_2$, and $Ge_2 - W_3$ distances have values of 1.39 ± 0.7 Å, whereas these same WFCs are closer to their respective

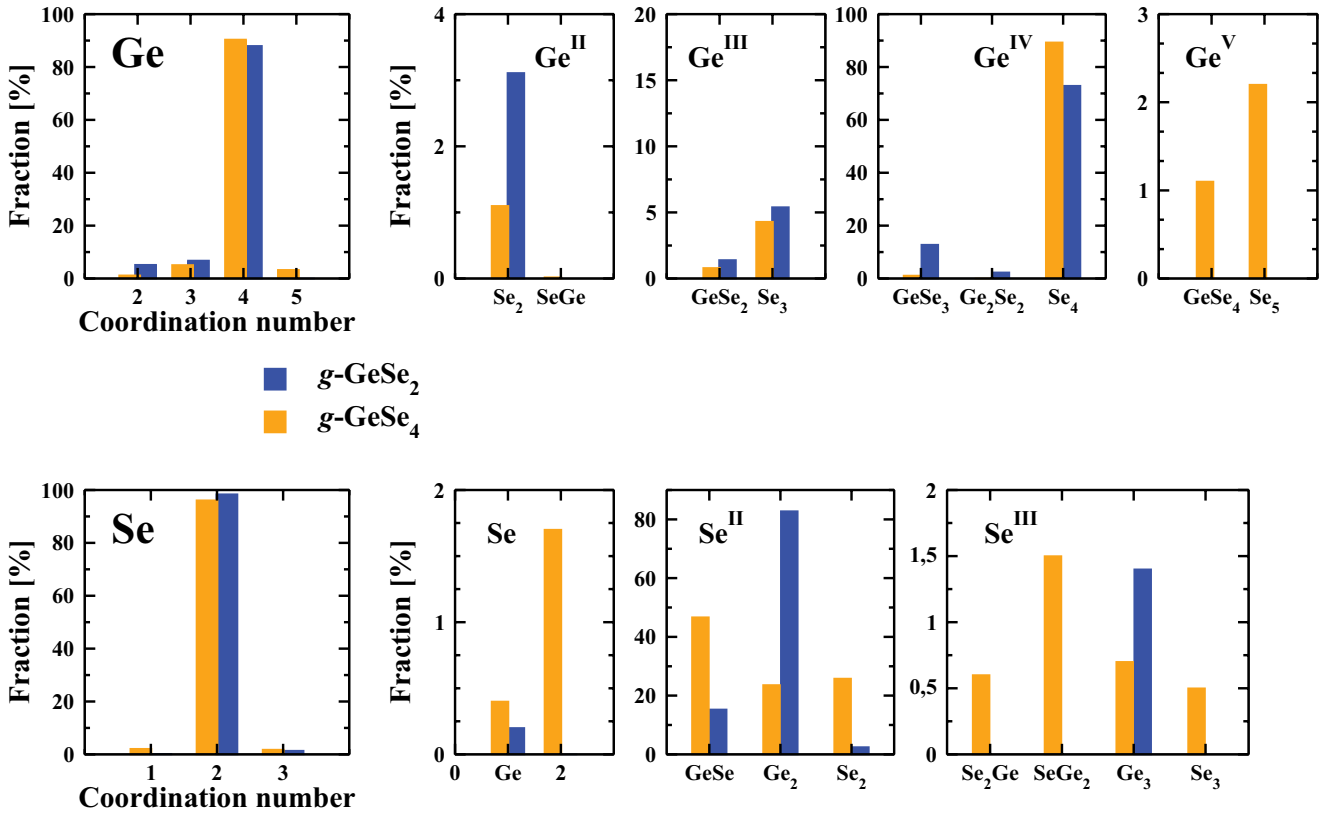

FIG. 7. (Color online) Percentage of l-fold coordinated atoms, also decomposed in term of each specific unit $\bar{n}_\alpha(l)$, for both Ge (top) and Se (bottom). The systems considered are g-$GeSe_2$ (in blue, from Ref. 26) and g-$GeSe_4$ (in orange, from Ref. 4).

Se atoms as much as 0.90 ± 0.4 Å, with W_1, W_2, and W_3 having comparable dispersions (2.45 ± 0.05 Å). The WFCs not participating to the bonding, such as W_5 in the left panel of Fig. 9, are located at distances of ∼0.41 Å from their closest Se atoms and the associated dispersion is around 2.45 Å. This is smaller than the dispersion characterizing the Ge DB discussed above. Both the tetrahedral-like location of these nonbonding WFCs and their dispersion closely resemble the lone pairs of oxygen in water systems, particularly, in the presence of ions close by.[40]

The above picture confirm the strong ionic contribution to Ge-Se bonding, pointing toward Se atoms as playing the role of electron acceptors, whereas the Ge atoms would be the corresponding donors. The fact that in a few cases electrons (WFCs) can be found in proximity of Ge atoms has to be interpreted as a transient phenomenon stemming from the bond formation processes. In fact, WFCs close to Ge are not present either in the right panel of Fig. 9 or in g-Ge_2Se_3 (see Fig. 10).

The right panel of Fig. 9 shows a Ge atom connected in a edge-sharing fashion, The Ge atom is visible at the center of the figure and labeled as Ge_1. In this particular snapshot, Ge_1 belongs to a four-fold ring carrying also Se_1 and Se_2, both of them having four WFCs in the typical tetrahedral arrangement discussed above. The bond which undergoes formation is Ge_1–Se_4, whose length is 2.56 Å, still rather long with respect to all the other Ge_1–Se bond distances (2.42–2.46 Å). For this reason, the WFC labeled as W_3 is found at comparable distances from both Ge_1 and Se_4, namely, $Ge_1 - W_3 = 1.33$ Å and $Se_4 - W_3 = 1.07$ Å, contrary to typical distances of ∼1.50 and ∼0.94 Å for Ge–WFC and Se–WFC, respectively, in regular Ge–Se bonds. Moreover, at variance with the other

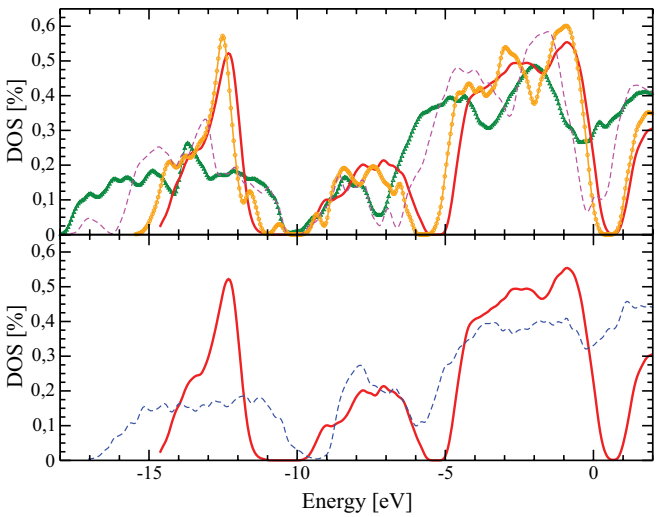

FIG. 8. (Color online) The electronic density of states extracted from the Kohn-Sham eigenvalues. (Top) Result for amorphous Ge_2Se_3 (solid red curve) is compared to that obtained for amorphous $GeSe_2$ (from Ref. 26, orange curve with circles), and amorphous $GeSe_4$ obtained using the PW (from Ref. 4 green curve with triangles) and the BLYP (broken pink curve) GGA functionals. (Bottom) Result for amorphous Ge_2Se_3 (solid red curve) is compared to that obtained for liquid Ge_2Se_3 (from Ref. 6, broken blue curve). A Gaussian broadening of 0.1 eV has been employed.

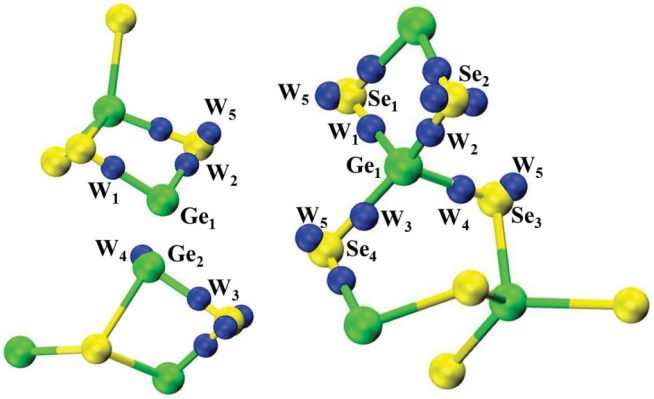

FIG. 9. (Color online) Details of the dynamically evolving structure in the liquid phase. The left panel shows the configuration that eventually leads to the formation of a homopolar bond Ge–Ge. The right panel shows the formation of an edge-sharing structure. Details are given in the text. Ge atoms appear in green, Se atoms in yellow, and the WFCs in blue.

WFCs (W_1, W_2, and W_4), W_3 is displaced slightly away from the bond axis joining the two atoms of 0.28 Å and its associated dispersion is 2.50 Å, slightly larger than the dispersion of W_1, W_2, and W_4 (2.44 Å). These features are typical of chemical bonds undergoing formation (or cleavage).[41] Once the Ge_1–Se_4 bond is formed, its length, WFCs locations, and related dispersions become identical to the other already formed Ge–Se bonds and contributed to the predominant tetrahedral unit of the amorphous network.

Both g-Ge_2Se_3 and l-Ge_2Se_3 lie in the rich Ge side of the composition range for the Ge_xSe_{1-x} network family. This means that the excess Ge atoms (i.e., those for which no Se atoms are available to form tetrahedral connections) have to form homopolar connections whenever no viable, i.e., energetically more accessible, alternatives exist. This is the case shown in Fig. 10 that refers to g-Ge_2Se_3. The left panel shows a typical Ge–Ge homopolar bond. The Se atoms labeled as Se_1, Se_2 and Se_3 are bound to Ge_1 in a typical arrangement not too dissimilar to the one considered in the case of the liquid. Namely, the WFCs W_2, W_3, and W_4 are closer to their corresponding Se atoms and their distances are all around

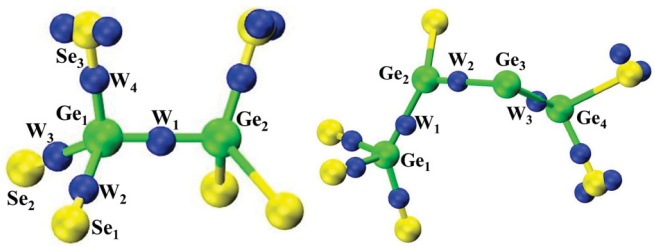

FIG. 10. (Color online) Details of homopolar bonds in the solid amorphous phase. The left panel shows a typical configuration with a single homopolar bond Ge–Ge. This is practically the final state with respect to the left panel of the former figure. The right panel shows a sequence of three homopolar bonds, which represent a peculiar, although not so frequent, structure of the vitreous system. Color codes are identical to the former figure: Ge in green, Se in yellow, and WFCs in blue. Details are given in the text.

~0.94 Å, with spread values of ~2.44 Å. The same holds for their counterparts on the Ge_2 side. More interestingly, the WFC labeled as W_1 is located in the middle of the Ge_1–Ge_2 bond ($Ge_1 - W_1 = 1.19$, $Ge_1 - W_1 = 1.22$ Å) and is characterized by a spread of 2.56 Å. This is the typical signature of a fully covalent single bond.[41]

Another interesting feature, again induced by the excess of Ge atoms, is the one reported in the right panel of Fig. 10. In this particular region of the network, there exists a chain of four Ge atoms chemically bonded to each other. This uncommon feature is accompanied by a specific local electronic structure that, in a sense, reflects the peculiarity of this bonding environment. A first feature we noticed is that not all the Ge–Ge bonds are equivalent. This seems to depend on the number and orientation of the extra "regular" Ge–Se bonds that the system is able to create. Specifically, in this four-member chain, the bond lengths are $Ge_1-Ge_2 = 2.50$, $Ge_2-Ge_3 = 2.54$, and $Ge_3-Ge_4 = 2.48$ Å. These inequalities are related to the fact that Ge_1 is bonded to three Se atoms, Ge_2 to one Se atom, Ge_3 has no Se bonded to it and finally Ge_4 forms two other bonds with Se atoms. In turn, the Ge–WFCs distances are as follows: $Ge_1 - W_1 = 1.06$ Å, $Ge_2 - W_1 = 1.44$ Å, $Ge_2 - W_2 = 1.01$ Å, $Ge_3 - W_2 = 1.53$ Å, $Ge_3 - W_3 = 1.60$ Å, and $Ge_4 - W_3 = 0.90$ Å. The spreads of the three WFCs, from the first to the third, are 2.67, 2.79, and 2.85 Å, respectively. In this respect, Ge_3, which turned out unable to bind to nearby Se atoms, is the more ionic member of the chain, having very large separations from the closest WFCs. Nonetheless, W_2 and W_3 are also characterized by larger dispersions, both with respect to W_1 and to all the other WFCs discussed in the former cases, underscoring again the peculiarity of such a bonding environment. Yet, the chain is stable at least on the time scale of the simulations and represents a specific feature in the case of an excess of Ge atoms in the glass formation process.

VII. CONCLUSION

The main purpose of this study was to understand the structural changes occurring in the disordered network Ge_2Se_3 when the liquid is quenched to form a glass. A previous set of data on l-Ge_2Se_3 is exploited to provide initial configurations for the cooling process, while making possible an accurate comparison between the two disordered phases. As a byproduct, the availability of a glass model for Ge_2Se_3 allows to analyze the changes in real and reciprocal space when spanning a range of concentrations within the Ge_xSe_{1-x} family of glasses. To this purpose, we took advantage of previous (and also partially updated results) on g-$GeSe_4$ and g-$GeSe_2$. In reciprocal space, the effect of cooling l-Ge_2Se_3 is an increase in the peak intensities, especially in the FSDP region for $S^{FZ}_{GeGe}(k)$. When the comparison is extended to the three glasses g-Ge_2Se_3, g-$GeSe_2$ and g-$GeSe_4$, changes in the relative intensities of the two first two peaks are found, the highest ratio between the FSDP and the main peak existing in g-Ge_2Se_3. From the standpoint of the Bhatia-Thornton formalism, the presence of a small feature in the FSDP region of $S_{CC}(k)$ for l-Ge_2Se_3, g-Ge_2Se_3, and g-$GeSe_2$ is indicative of a moderate departure from chemical order. Further information

on chemical order has been extracted from the partial pair distribution functions. The systems considered share two main features: (a) a three peaks pattern at $r < 5$ Å in $g_{GeGe}(r)$, due to the presence of homopolar Ge-Ge bonds, edge-sharing, and corner-sharing connections and (b) a very intense maximum at the location of Ge-Se first-neighbor interatomic distances. In the former case (a), the intensities of the three peaks are strongly dependent on the composition. This is particularly true for the first peak that vanishes in the g-$GeSe_4$ case, becomes noticeable in the g-$GeSe_2$ case, and it is very intense in g-Ge_2Se_3, as a result of Ge−Ge homopolar bonds. Partial coordination numbers are indicative of a strongly predominant tetrahedral network for all compositions and result in total coordination numbers consistent with the "$8 - N$" rule. Among all disordered networks, g-$GeSe_4$ is the one exhibiting the highest degree of chemical order. Looking at the structural units, it is of interest to underline the reduction of twofold coordinated Ge atoms occurring from the liquid to the glass Ge_2Se_3. We have rationalized this reduction by invoking the inability for certain Ge pairs of atoms to surmount energetic barriers at low temperature and form homopolar bonds, thereby preferring (whenever available) the most stable tetrahedral configurations.

The electronic structure character of g-Ge_2Se_3 and l-Ge_2Se_3 has been highlighted through the calculation of the electronic density of states, which reveals an enhanced gap opening in the glass. We were also able to provide clear-cut evidence on the effect of the exchange-correlation functional on the electronic density of states of $GeSe_4$. In the vicinity of the Fermi level (and in the context of a comparison carried out with the same exchange-correlation functional, BLYP), the shape of the EDOS for the glassy networks g-Ge_2Se_3, g-$GeSe_2$, and g-$GeSe_4$ is similar, the larger gap being recorded for g-$GeSe_2$. We have taken advantage of the localized description of bonding in terms of the Wannier functions and centers to describe specific bonding patterns involving either Ge-Ge homopolar or Ge-Se heteropolar connections, respectively. In particular, the position of the Wannier centers and their spread allows to distinguish between dangling (undercoordinated Ge atoms), ionocovalent (Ge−Se bonds in tetrahedra), and covalent (Ge−Ge homopolar) bonds. Overall, the present work contributes to achieving a more complete understanding of the structure of g-Ge_xSe_{1-x} systems by pointing out under which conditions of compositions and why the regularity of the predominant tetrahedral network is altered by the presence of miscoordinations and homopolar bonds.

ACKNOWLEDGMENT

This work was granted access by GENCI (Grand Equipement National de Calcul Intensif) under allocation 2011095071 to the HPC resources of CCRT/CINES/IDRIS.

[1] P. S. Salmon, J. Non-Cryst. Solids. **353**, 2959 (2007).
[2] C. Massobrio, A. Pasquarello, and R. Car, Phys. Rev. B **64**, 144205 (2001).
[3] C. Massobrio and A. Pasquarello, Phys. Rev. B **77**, 144207 (2008).
[4] C. Massobrio, M. Celino, P. S. Salmon, R. A. Martin, M. Micoulaut, and A. Pasquarello, Phys. Rev. B **79**, 174201 (2009).
[5] M. Micoulaut, R. Vuilleumier, and C. Massobrio, Phys. Rev. B **79**, 214205 (2009).
[6] S. Le Roux, A. Zeidler, P. S. Salmon, M. Boero, M. Micoulaut, and C. Massobrio, Phys. Rev. B **84**, 134203 (2011).
[7] M. Micoulaut, S. Le Roux, and C. Massobrio, J. Chem. Phys. **136**, 224504 (2012).
[8] X. Zhang and D. A. Drabold, Phys. Rev. B **62**, 15695 (2000).
[9] M. Durandurdu and D. A. Drabold, Phys. Rev. B **65**, 104208 (2002).
[10] M. M. G. Alemany and J. R. Chelikowsky, Phys. Rev. B **68**, 054206 (2003).
[11] D. N. Tafen and D. A. Drabold, Phys. Rev. B **68**, 165208 (2003).
[12] D. N. Tafen and D. A. Drabold, Phys. Rev. B **71**, 054206 (2005).
[13] A. D. Becke, Phys. Rev. A **38**, 3098 (1988).
[14] C. Lee, W. Yang, and R. G. Parr, Phys. Rev. B **37**, 785 (1988).
[15] R. Car and M. Parrinello, Phys. Rev. Lett. **55**, 2471 (1985).
[16] C. Massobrio, M. Micoulaut, and P. S. Salmon, Solid State Sci. **12**, 199 (2010).
[17] M. Micoulaut and C. Massobrio, J. Optoelect. Adv. Mat. **11**, 1907 (2009).
[18] J. P. Perdew and Y. Wang, Phys. Rev. B **45**, 13244 (1992).
[19] N. Troullier and J. L. Martins, Phys. Rev. B **43**, 1993 (1991).
[20] S. Nosé, Mol. Phys. **52**, 255 (1984).
[21] W. G. Hoover, Phys. Rev. A **31**, 1695 (1985).
[22] P. E. Blöchl and M. Parrinello, Phys. Rev. B **45**, 9413 (1992).
[23] N. Marzari and D. Vanderbilt, Phys. Rev. B **56**, 12847 (1997).
[24] R. Resta and S. Sorella, Phys. Rev. Lett. **82**, 370 (1999).
[25] P. S. Salmon and J. Liu, J. Phys.: Condens. Matter **6**, 1449 (1994).
[26] A. Bouzid and C. Massobrio, J. Chem. Phys. **137**, 046101 (2012).
[27] A. B. Bhatia and D. E. Thornton, Phys. Rev. B **2**, 3004 (1970).
[28] H. E. Fischer, A. C. Barnes, and P. S. Salmon, Rep. Prog. Phys. **69**, 233 (2006), describe the relationship between the three sets of partial structure factors commonly used (Faber-Ziman, Ashcroft-Langreth, and Bhatia-Thornton).
[29] P. S. Salmon and I. Petri, J. Phys.: Condens. Matter **15**, S1509 (2003).
[30] C. Massobrio, M. Celino, and A. Pasquarello, Phys. Rev. B **70**, 174202 (2004).
[31] L. Giacomazzi, C. Massobrio, and A. Pasquarello, Phys. Rev. B **75**, 174207 (2007).
[32] C. N. J. Wagner and H. Ruppersberg, Atomic Energy Rev. **1**, 101 (1981).
[33] P. Chieux and H. Ruppersberg, J. Phys. Coll. **41**, C8 (1980), discuss the case when $S_{NC}(k) = 0$, which corresponds to $g_{NC}(r) = 0$. Then $c_{Ge}g_{GeGe}(r) + c_{Se}g_{GeSe}(r) = c_{Se}g_{SeSe}(r) + c_{Ge}g_{SeGe}(r)$ for all r values and $\bar{n}_{Ge} = \bar{n}_{Se}$ such that the generalized Warren-Cowley short-range chemical order parameter reduces to the more usual expression $\alpha'_w = 1 - \bar{n}_{GeSe}/c_{Se}\bar{n} = (4\pi\, n_0/\bar{n}) \int_{r_1}^{r_2} dr\, g_{CC}(r) r^2$, where r_1 and r_2 denote the minima on either side of the first peak in $g_{CC}(r)$. Since $g_{CC}(r) = c_{Ge}c_{Se}\,[g_{GeGe}(r) + g_{SeSe}(r) - 2g_{GeSe}(r)]$, a preference for heteropolar bonds corresponds to $\alpha'_w < 0$, whereas a preference for homopolar bonds corresponds to $\alpha'_w > 0$.
[34] G. S. Cargill III and F. Spaepen, J. Non-Cryst. Solids. **43**, 91 (1981).

[35]M. Maret, P. Chieux, P. Hicter, M. Atzmon, and W. L. Johnson, J. Phys. F **17**, 315 (1987).
[36]M. J. Haye, C. Massobrio, A. Pasquarello, A. De Vita, S. W. De Leeuw, and R. Car, Phys. Rev. B **58**, R14661 (1998).
[37]F. H. M. van Roon, C. Massobrio, E. de Wolff, and S. W. de Leeuw, J. Chem. Phys. **113**, 5425 (2000).
[38]R. A. Street, R. J. Nemanich, and G. A. N. Connell, Phys. Rev. B **18**, 6915 (1978).
[39]K. Tanaka, Phys. Rev. B **39**, 1270 (1989).
[40]R. Scipioni, D. A. Schmidt, and M. Boero, J. Chem. Phys. **130**, 024502 (2009).
[41]M. Boero, M. Parrinello, S. Huffer, and H. Weiss, J. Am. Chem. Soc. **122**, 501 (2000).